Article

MMS

Mathematics and Mechanics of Solids
1–11

DOI: 10.1177/10812865221124142
journals.sagepub.com/home/mms

The effect of pore sizes on the elastic behaviour of open-porous cellular materials

Shivangi Aney and Ameya Rege
Department of Aerogels and Aerogel Composites, Institute of Materials Research, German Aerospace Center (DLR), Cologne, Germany

Received 9 March 2022; accepted 19 August 2022

Abstract
The influence of the pore structure characteristics in open-porous cellular materials on their macroscopic elastic behaviour is investigated by considering three important microstructural features *viz*. the relative density, the pore-size distribution, and the pore-wall thickness. To this end, a microstructure-informed modelling approach is presented, where all elements of the three-dimensional (3-d) pore structure can be controlled effectively. The results show that while density does dictate the mechanical properties of open-porous solids, the effects of the pore-wall thickness and the pore-size distribution are not negligible and must be considered while developing such materials, in particular those that exhibit a poly-disperse nature and require load-bearing capabilities under finite strains.

Keywords
Open-porous materials, Laguerre-Voronoi tessellations, relative density, pore-size distribution, pore-wall thickness, macroscopic mechanical properties

1. Introduction

There has been a profound interest in the mechanical properties of open-porous cellular materials, particularly because of their high strength-to-weight ratios and their ubiquitous appearance in nature, for example, in human bones, plant stems and marine sponges as well as due to the ability to mimic this porous structure in the synthesis of man-made materials, for example, ceramics, polymers, metal foams, and aerogels [1–3]. These materials are lightweight, multi-functional and as a result show high demand in numerous applications [4–9]. Nanoporous cellular materials are leading candidates for thermal insulation applications due to their exceptionally low thermal conductivities [10]. However, there is often a trade-off while maximising the mechanical stiffness of the cellular solid while maintaining a low thermal conductivity. This is because both these properties are dependent, among others, on the solid fraction. This presents a challenge to develop multifunctional open-porous materials for thermal superinsulation applications. In particular, to improve the mechanical stability and properties of the materials for targeted applications, an in-depth understanding of the open-porous microstructure and its influence on

Corresponding author:
Ameya Rege, Department of Aerogels and Aerogel Composites, Institute of Materials Research, German Aerospace Center (DLR), Linder Höhe, Cologne 51147, Germany.
Email: ameya.rege@dlr.de

the macroscopic mechanical response is preeminent. This is reflected by an increasing research interest in the investigations on the characteristics of pore-sizes and pore-size distributions and their subsequent influence on the properties of open-porous cellular materials. Lutz and Zimmerman [11] reviewed the effects of the pore shape on the Poisson ratio of porous materials. Idealised pore shapes, for example, circular, square and triangular in two-dimensions (2-d), were used to investigate this effect. Langlois et al. [12] studied the modifications in the permeability of solid foam due to membrane obstructions, thus investigating the effect of pore connections. Song et al. [13] proposed an algorithm for estimating the pore-size distribution from discrete digital images of porous networks, while Hertel et al. [14] presented the magnetic-resonance pore imaging of non-symmetric microscopic pore shapes. Furthermore, Bakhshian and Sahimi [15] studied the effect of deformation on the morphology and flow properties of porous media using extensive computer simulations.

From a theoretical and computational perspective, the heterogeneous and random pore shape and structure of foams and foam cells, and their corresponding topological and geometric properties have been computationally investigated using Voronoi tessellations [16,17]. The prediction of the elastic moduli of the complex microstructure of synthetic open-cell foams was studied with finite element models and demonstrated good accuracy [18]. The efficacy of these models was further demonstrated by incorporating the key geometric characteristics of real foams into the analysis. Moreover, it was shown that the foam strength calculated based on these models compared well with experimental results despite the different localised microstructural deformations. This led to the conclusion that the randomness of the actual microstructure plays a secondary role in the case of mono-disperse foams [18,19]. While this may hold true, the assumption was also applied to porous materials showing a poly-disperse nature. However, the situation can be very different in this case, as the actual microstructure may play a rather important role. For example, in the case of 2-d Voronoi honeycombs, it was shown that as the cell irregularity increases, the effective Young's modulus and shear modulus increase, while the bulk modulus decreases, for a constant relative density [20]. The influence of cell irregularity under high-strain compression for low relative density (solid fraction = 0.08) has also been analysed by quantifying cell irregularity with a regularity parameter [21].

Such 2D Voronoi-based models of open-porous materials have shown to be insensitive to differences in the random generation of seed points [22]. This check becomes very important for the applicability of such models to describe the behaviour of real materials. Li et al. [23] demonstrated the effects of varying the cell shape and cross-sectional area on the elastic properties of 3-d open-cell foams revealing important insights and considerations for computationally modelling the open-porous microstructure. The validity of such computational models is then generally proven by comparing their results with experimental data. However, there are two major challenges to experimentally investigate purely the influence of the pore-structure and pore-size distribution. First, it is very difficult to tune only the pore-size distribution experimentally while synthesising an open-porous material, keeping all other parameters constant. Hence, a theoretical or computational approach is more suitable. Second, most micro-mechanical models [24–26] developed to predict the material properties are based on an idealised pore-shape (2-d or 3-d), whereas in reality, the pore shape is random.

In this paper, these challenges are addressed by utilising a theoretical approach to study the effect of the pore space on the mechanical response of the macroscopic material. To achieve this goal, the identification of key microstructural quantities that play a significant role is important. These are, the relative density of the solid, the pore-size distribution (particularly important for poly-disperse foam-like materials), and the pore-wall thickness [25]. By targeting these three factors, an attempt to qualitatively as well as quantitatively answer whether pore-sizes and shapes really have an influence on the mechanical properties of cellular solids is made. This is an extension to our previous work in which the influence of the mean pore-size and the broadness of the pore-size distribution on the macroscopic mechanical response was analysed by proposing a generalised micromechanical constitutive model [25].

2. Computational modelling

Our modelling approach uses the concept of a representative volume element (RVE) which is chosen to be representative of the microstructure of the material. Then, simulating the RVE by defining periodic boundary conditions results in simulating the bulk behaviour of the material. The concept of RVE is

generally applied in multiscale simulations, wherever the information from the microstructural deformation in the material's network becomes necessary [27,28] as is the case in our study. For poly-disperse open-porous materials, it is expected based on our previous results [25] that the material heterogeneity due to the variation in the pore-sizes must have an influence on the material properties. Hence, the specified multiscale modelling approach is opted. It is imperative to choose the correct RVE size in order to avoid the size effects which may arise if the chosen RVE is not sufficiently large. Different methods [29–33] to determine the RVE size, for example, experimental, statistical or numerical depending upon the application can be implemented. In our study, the RVE size could not be estimated from experimental data as not one particular material is being investigated in this study. Thus, based on our previous work [34], a sufficiently large RVE encompassing the given pore-size distribution is chosen. This becomes particularly important for poly-disperse network structures. More information on the choice of RVE size is provided below.

The process of reconstructing the 3-d open-porous network is described as follows and is also sketched in Figure 1. First, a fully periodic random dense packing of poly-disperse spheres is created with the pore-size distribution as an input, where the poly-disperse spheres represent the pores varying in sizes. The important parameters necessary here are the pore-size distribution and the total number of pores (spheres in this case). Generation of such random sphere packs has been widely used to understand the microstructure of porous solids and their bulk properties [15,34–36]. The dense sphere-packing can be created using various sequential or rearrangement models based on different generation algorithms [36,37]. Baranau et al. [38] and Chandrasekaran et al. [34] have compared four different sphere-packing algorithms *viz*., force-biased algorithm [39], Lubachevsky-Stillinger [37] algorithm (LS), Lubachevsky-Stillinger algorithm with gradual densification (LSGB), and Lubachevsky-Stillinger algorithm with equilibrium between compressions (LSEBC), where the latter compared them for modelling the pore-size distributions of κ-carrageenan aerogels, and concluded that although all algorithms were verified and showed good agreement with experiment data, the LS algorithm was computationally 10 times faster in comparison to LSEBC. Hence, the LS algorithm has been used in our work. Baranau et al. [38,40] have provided important insights regarding the use and parameter sensitivity of the event driven simulation-based Lubachevsky-Stillinger algorithm [37] by introducing a method to calculate the pore-size entropy. While the generated sphere packs adhere to the necessary pore-size distributions, this step alone is not sufficient to describe the open-porous microstructure of the material. Hence, we introduce the Voronoi tessellation onto the generated sphere packs. A Voronoi tessellation [41] can be described as partitioning of space into a number of distinct regions based on the corresponding points included in that space. The partitioning is done such that each region R_i referred to as a Voronoi cell, represents the subset of the domain which is closer to the corresponding seed S_i than to any other seed S_j. In mathematical terms, a point x is a part of a Voronoi cell i with nucleus r_i iff:

$$||x - r_i||^2 < ||x - r_j||^2 \quad \forall j \neq i. \tag{1}$$

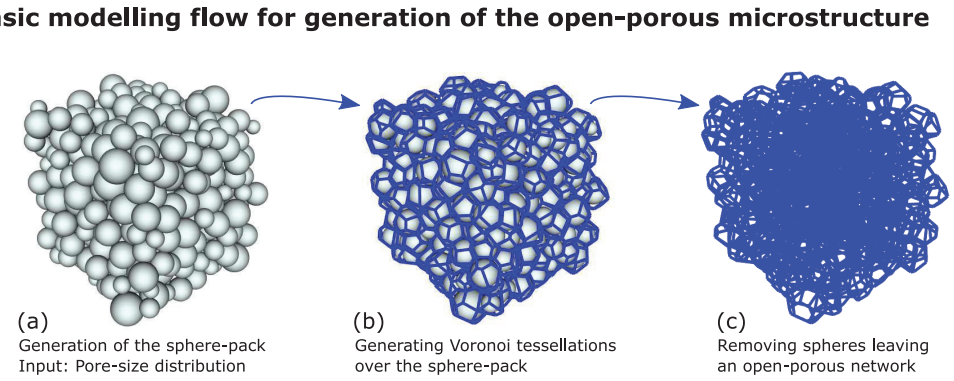

Figure 1. Schematic illustration of the process of generating a 3-d representative volume element (RVE) based on any given pore-size distribution: (a) Generating a sphere packed simulation box, (b) constructing Laguerre-Voronoi Tessellation on the spheres, (c) removing spheres leaving an open-porous network.

There are different methods of generating these Voronoi geometries based on location and generation of the seed points, thus resulting in different overall Voronoi structures. For example, in the case of random arrangement of seed points without relaxation, the Voronoi geometry generated often has pointed and sharp cells, while relaxation leads to a rather mono-disperse Voronoi geometry. To generate poly-disperse Voronoi structures, the Laguerre-Voronoi tessellation is suitable [42]. Although the Laguerre-Voronoi tessellation uses a similar concept for partitioning of 2-d or 3-d space, the desired cell size is specified additionally along with the cell coordinates. Thus, the initial cell can be represented by a circle (in 2-d) or a sphere (in 3-d) with the centre coordinates and the radius as the cell size. Mathematically, a point x is a part of a Laguerre Voronoi cell i with nucleus r_i iff:

$$||x - r_i||^2 - {R_i}^2 < ||x - r_j||^2 - {R_j}^2 \quad \forall j \neq i, \tag{2}$$

where R_i represents the size of the ith cell. Alsayednoor and Harrison [43] evaluated the performance of using different types of Voronoi tessellations for microstructure generation in 2-d. Although attempts have been made to study the structure-property relationships with a simple Voronoi geometry [44], a Laguerre-Voronoi approach seems more successful and suitable [34,43]. In our work, the sphere packing was generated from the pore-size distribution using the random close packing of poly-disperse spheres (RCPPS) algorithm (see Figure 1(a)). This served as the input for generating the Laguerre-Voronoi tessellation as shown in Figure 1(b). Subsequently, the closed pore space represented by the sphere pack is converted to an open-porous skeletal network as shown in Figure 1(c). The Laguerre-Voronoi geometry can generate a relatively realistic fully isotropic RVE representing poly-disperse porous microstructures [43]. These RVEs consist of polyhedral cells with their edges representing the pore-walls of the cellular solid. However, it can be observed that the new cell volumes are larger than the initial sphere pack volumes. Thus, to ensure an exact congruence of the input pore-size distribution with the volume distribution of the Voronoi cells, the initial sphere packing is scaled accordingly. Finally, this Laguerre-Voronoi geometry is translated in the x, y and z directions and cut into a cube shaped RVE maintaining its periodicity. Moreover, the choice of the RVE size becomes important. In our case, this depended on two factors. First, how accurately the pore-size distribution can be approximated with the sphere-pack and second, the convergence of the macroscopic material response. Hence, in our case, the RVE size closely relates to the number of spheres in the sphere-pack generated for a given pore-size distribution. After carefully evaluating RVEs with sizes of 50, 100, 200, 500 and 3000 spheres, it was realised that the approximation of pore sizes and the resulting mechanical behaviour coalesced for RVEs sized 500 spheres and above. Thus, a sphere-pack of 500 spheres was chosen for all simulations.

Within the framework of multiscale modelling, it is desired to simulate the RVE, representing the microstructure, in a way that the macroscopic material properties can be determined. Thus, the finite element methods have been used as a tool here to simulate the bulk properties of the materials. The edges of the pores (cells) in the RVE representing pore-walls are modelled as beam elements (B31—linear beam element in Abaqus) with a circular cross-section. Modelling the cell walls based on the beam theory is well known in the cellular materials community [24,45–47]. These edges correspond to the pore-walls, and the diameter to their thickness. This cross-section was randomly chosen and the use of different cross-sections can be adopted without introducing complexity in the models. The RVEs are then simulated in Abaqus under uniaxial compressive loading. The open-porous cellular network with low relative density allows the use of structural beam elements instead of continuum elements [43]. The use of periodic boundary conditions helps to obtain a homogenised macroscopic mechanical response, as it constrains the degrees of freedom of the periodic boundary nodes, thus preserving stress continuity across the boundary [28]. The process of applying such periodic boundary conditions for an RVE has been described by Wu et al. [48]. This concept of constraining the periodic boundary nodes and applying the loads on dummy nodes has been implemented. Geometric nonlinearity was activated in the finite element model.

To realise the aim of investigating the influence of the three parameters, *viz*. the relative density, the pore-size distribution, and the pore-wall thickness, two use-cases were defined with the intention of investigating purely the effect of the pore-wall thickness and the relative density on the macroscopic material properties. It was previously shown that the variation in the mean of the pore-size distributions shows a rather significant influence on the mechanical properties as compared to the variation in the

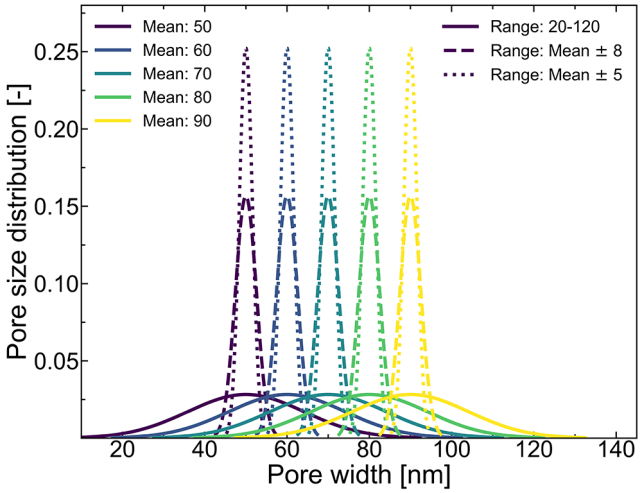

Figure 2. Pore size distributions considered for each use case. There are fifteen total distributions, comprising of five median values and three standard deviations.

Table 1. Simulation parameters for the use-cases 1 and 2. Consistent units have been used throughout.

	Use-case 1	Use-case 2
Parameter of interest	Pore-wall thickness	Relative density
Parameter values	3, 5, 7	0.08, 0.1, 0.15
Median values of pore-size distributions	50, 60, 70, 80, 90	
Range of pore-size distributions	20-120, mean ±8, mean ±5	
No. of simulations	45	

standard deviation [25]. Hence, for this study, we considered five mean pore-width values and three standard deviations corresponding to different ranges of the pore-size distributions. This resulted in a total of 15 different distributions for each use-case (see Figure 2 and Table 1). In this work, normal distribution functions were chosen to describe the variation in the pore sizes. The mean corresponds to the median value of the chosen function, thus providing information of the peak pore-width of the pore-size distribution. Here, the pore-width represents the width of the cell. The standard deviation corresponds to the dispersion in the range of the pore-size distribution. For example, the pore-size distribution, for any given mean, with a range of 20–120 shows a very broad standard deviation compared to the one having a narrow range of mean ±5. For example, for a mean pore-width of 60, the distribution with a range of 20–120 will have a broader dispersion than in the case of one with 55–65, as illustrated in Figure 2. These values were determined depending on the intended applicability of the computational approach. As an example, we consider three standard deviation values for the distributions to include both conventional foam-like materials [49] which do not show intensive pore-size variations, as well as nanoporous materials like aerogels which boast a large pore-size variation, for example, from 2 nm to 100 nm [47].

In the first use-case, the pore-wall thickness was fully controlled and maintained at 3, 5 and 7, while for a given pore-wall thickness, the effect of varying the mean pore-width and the standard deviation on the elastic behaviour was analysed. Here, no control was maintained over changes to the relative density. Thus, considering five mean values, three standard deviations resulting in different ranges of the pore-size distributions and three parameter values, we simulated 45 material responses for this case. On the other hand, in the second use-case, the relative density was controlled but not the pore-wall thickness. The relative density was maintained at 8%, 10% and 15% for the three different standard deviations and five different means, resulting again in a total of 45 simulations. The limitation of these two use-

cases was that at any given instance, one parameter remained uncontrolled. To overcome this issue, a third use-case was defined, wherein all the three parameters, *viz*., the pore-size distribution, the pore-wall thickness as well as the relative density were controlled. All data were generated in triplicate to ensure accuracy and eliminate process bias. In this paper, only averaged data are plotted as the statistical variations in the data were insignificant ($<0.01\%$). Also, consistent units were used, such that the results can be replicated for pore sizes in different scales. Here, one must note that while replicating these results for pore sizes in different scales, care has to be taken concerning the relevance of surface effects. This has not been accounted for in the presented model.

3. Results and discussion

This section elucidates the results obtained from analysing the effect of different parameters of the pore-size distributions on the macroscopic mechanical properties. First, the microstructural deformation of the RVE can be visualised. The RVE in the reference configuration as well as in the deformed one for one of the simulations is shown in Figure 3. Here, the RVE was subjected to uniaxial compression of 10%. The results of the first use-case are illustrated in the Figure 4. In the first use-case, the pore-wall thickness was varied from 3 to 7 units and the mean pore-width was varied from 50 to 90 units. Figure 4(a)–(f) represent results for RVEs with pore sizes having ranges between mean ± 5 and mean ± 8, respectively, while Figure 4(g)–(i) shows results for RVEs having pore sizes ranging from 20 to 120 units. For all the different pore-wall thicknesses, it can be observed that, for any given pore-space, the lower the mean pore-size, the stiffer was the mechanical response. This was observed in each sub-plot and it echoes the results from our previously published micromechanical constitutive model [25].

An important point to note here is that narrower pore-size distributions, such as in Figure 4(a)–(f) show enhanced stiffening with lowering of the mean pore-widths compared to the ones shown in Figure 4(g)–(i) which have a wider pore space. Previously, it was established that conventional foams, characterised by small variations in the pore-sizes, do not show pore-size dependency. However, our simulations suggest a pore-size dependency even for variations in the pore-sizes of ± 5 units considering purely the effect of the pore-wall thickness on the stress-strain response. Here, one must not conflict between cell irregularity and cell-size distribution. The properties show negligible sensitivity with changes to the former but that is not the case with the latter. Note that while the pore-wall thickness was kept constant, the relative density was not controlled in this use case. Thus, for a given pore-wall thickness, with increasing mean pore-width, the solid fraction decreased. For the pore-wall thickness of 3 units, while the mean pore-width increased from 50 to 90 units, the solid fraction decreased from 4.6% to 1.4% for the pore-size distribution range of mean $\pm$ 5 and mean $\pm$ 8 and the solid fraction decreased from 3.9% to 1.3% for the wider pore-size distribution with a range of 20 to 120 units. Similarly, in case of the pore-wall thickness of 5 units, while the mean pore-width increased from 50 to 90 units, a decrease in the solid fraction from 12.87% to 3.9% for the pore-size distribution range of mean $\pm$ 5 and mean $\pm$ 8 was observed and the solid fraction decreased from 10.81% to 3.75% for the

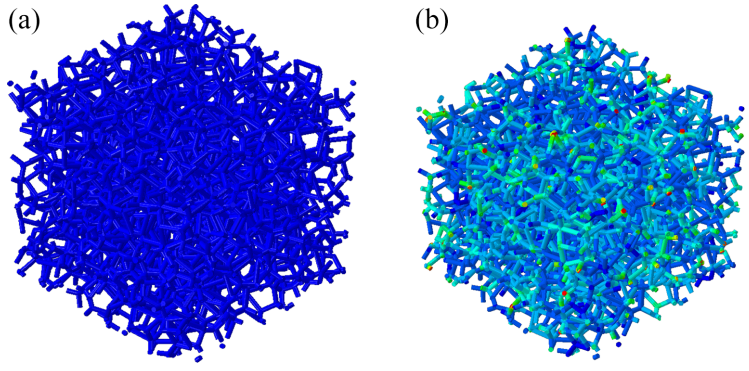

Figure 3. Illustration of the cube-shaped representative volume element (RVE). (a) RVE in the reference state and (b) RVE under uniaxial compression.

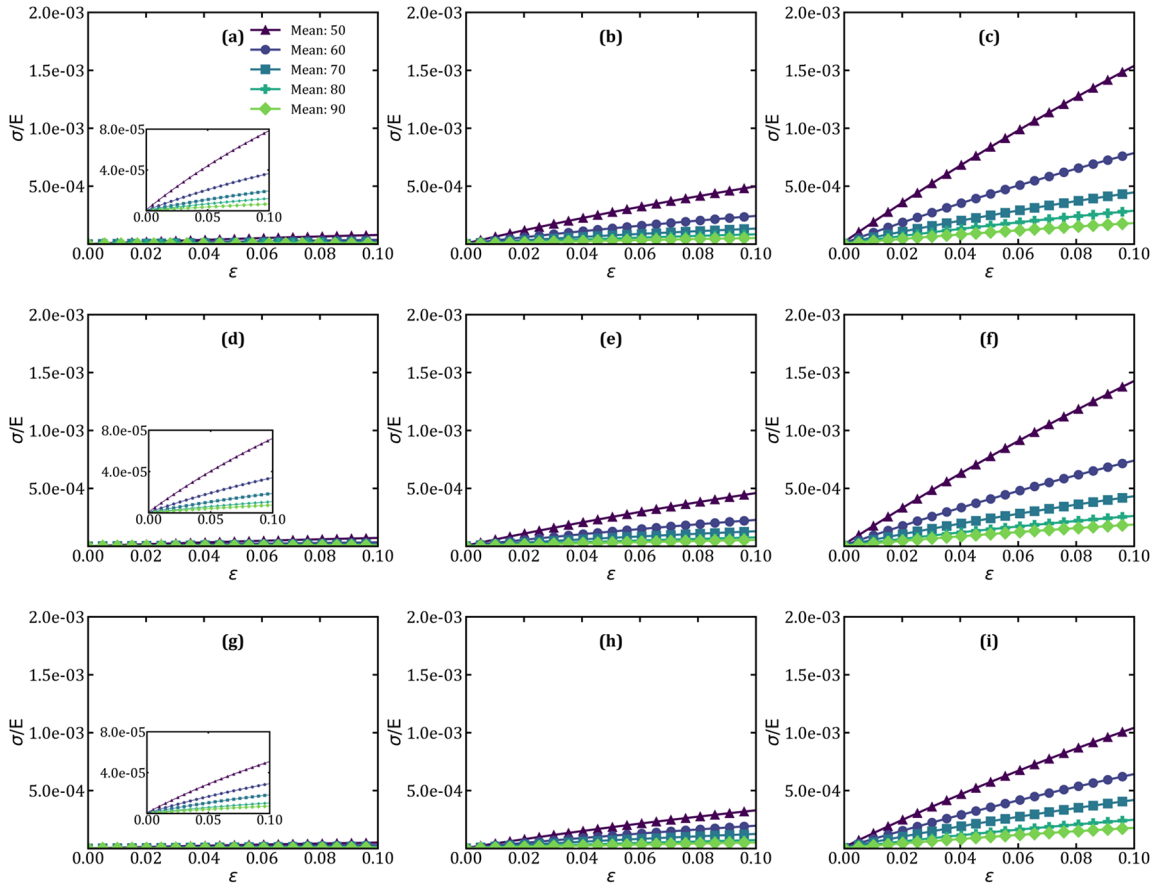

Figure 4. Effect of varying the mean pore-width on the macroscopic stress-strain response for open-porous material for a given pore-wall thickness. Range of pore sizes: mean ±5 units: pore-wall thickness (a) 3 units, (b) 5 units, (c) 7 units; range of pore sizes: mean ±8 units: pore-wall thickness (d) 3 units, (e) 5 units, (f) 7 units; range of pore sizes: 20–120 units: pore-wall thickness (g) 3 units, (h) 5 units, and (i) 7 units. Consistent units are used throughout in all simulations.

wider pore-size distribution with a range of 20 to 120 units. And finally, for the pore-wall thickness of 7 units, with a similar increase in the mean pore-width, the solid fraction decreased from 25.23% to 7.7% for the pore-size distribution range of mean ± 5 and mean ± 8 and from 21.2% to 7.3% for the wider pore-size distribution with a range of 20 to 120 units. Thus, with the varying solid fraction it was not possible to confidently conclude that the pore-wall thickness solely influences the mechanical response.

In the second use-case, as portrayed in Figure 5, the macroscopic mechanical response was studied subject to changes in the solid fraction. The scheme of Figure 5(a)–(i) is similar to that in 4 (a)-(i). However, in Figure 4, the pore-wall thickness was varied between 3 and 7 units, whereas in Figure 5, the solid fraction was varied between 8% and 15%. It can be seen, that for a constant solid fraction, the variations in the mean pore-sizes and the pore-size distributions do not show significant effect on the stress-strain response. However, it must be carefully analysed, that in order to maintain the solid fraction and pore-size distribution, the pore-wall thickness varied. Thus, in Figure 5, there was no control over the pore-wall thickness. Here, for a given solid fraction, with increasing mean pore-width, the pore-wall thickness increased. For example, for maintaining the solid fraction of 8%, the thickness increased from 4 to 7 units while increasing the mean pore-width from 50 to 90 units. Similarly, the thickness increased from 4.5 to 8 units while maintaining the solid fraction at 10% for increase in the mean pore-size. And in case of maintaining the solid fraction at 15%, the thickness increased from 5 to 10 units for a similar increase in the mean pore-size. Thus, even in this case, based on the presented results one cannot claim that the relative density has a sole influence on the macroscopic stress–strain response. From the above-mentioned two use cases, it can be realised that there is an interplay between

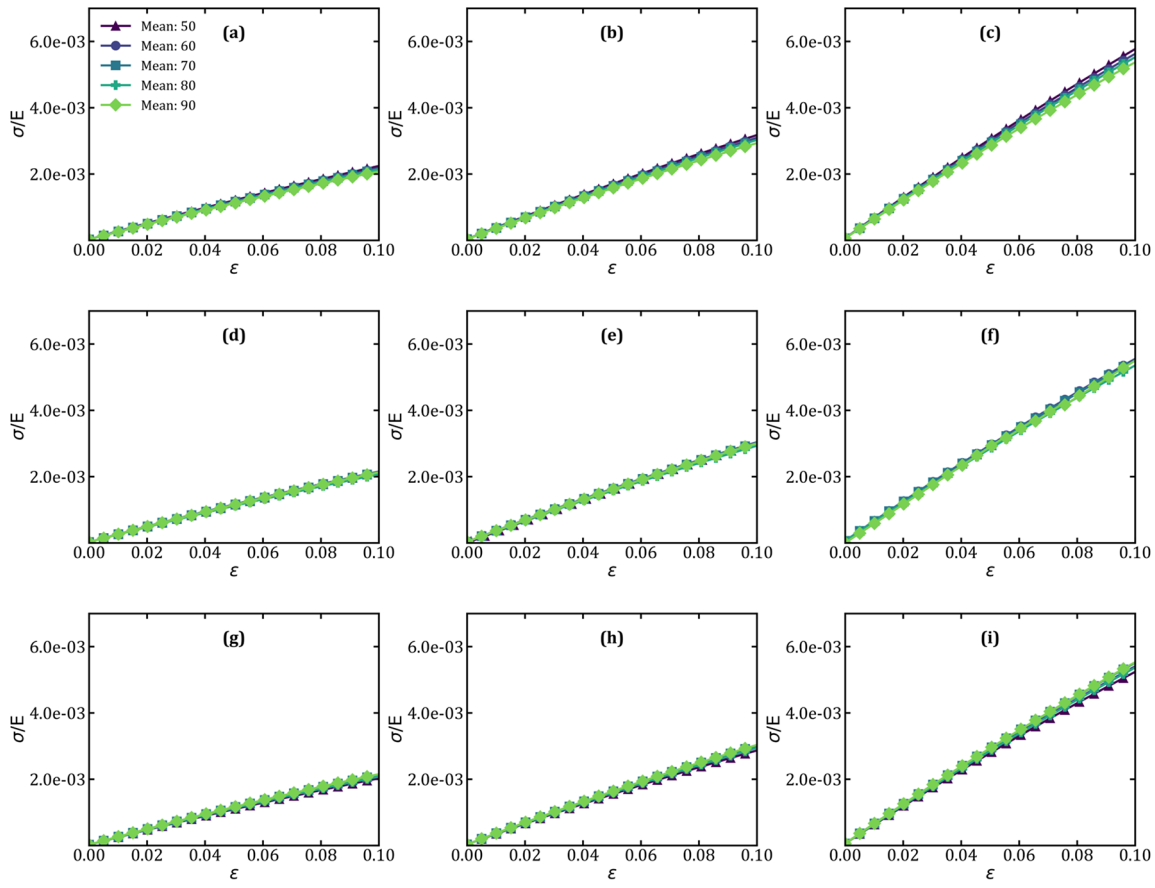

Figure 5. Effect of varying the mean pore-width on the macroscopic stress-strain response for open-porous material for a given solid fraction (relative density). Range of pore sizes: mean ±5 units: solid fraction (a) 0.08, (b) 0.1, (c) 0.15; range of pore sizes: mean ±8 units: solid fraction (d) 0.08, (e) 0.1, (f) 0.15; range of pore sizes: 20–120 units: solid fraction (g) 0.08, (h) 0.1, (i) 0.15. Consistent units are used throughout in all simulations.

the density and pore-wall thickness while dictating the bulk mechanical behaviour. To present a solution to this challenge, a third use-case was defined. Here, the solid fraction as well as the pore-wall thickness were controlled, that is, kept constant, and the pore-size distribution was varied with respect to their mean pore-width.

The results of the final use-case are illustrated in Figure 6. Here, the pore-wall thickness was defined at 3 units and the solid fraction was maintained at 2.5%. It can be observed again, that the lower the mean pore-width, the stiffer was the mechanical response. This also echoes the results from the first use-case, albeit the amplification in the stiffness was smaller when the solid fraction was parallely controlled. This stiffening can be observed even for the illustrated case, where by lowering the mean of the pore-size distribution from 70 units to just 60 units, while keeping all other quantities the same, a 6.7% increase in the stiffness of stress-strain curve was observed under finite strains. Such stiffening would be pronounced when the difference in the mean pore-widths becomes larger. Surely, the stiffening effect is much less pronounced in the linear elastic region. However, this may not be the case if the difference in the mean pore-sizes is considerable, for example, 60 and 150 units where one would expect a pronounced stiffening even in the linear elastic region. This must be investigated further. With the computational approach used in this analysis, it was difficult to control both the solid fraction as well as the pore-wall thickness. Hence, the mean pore-width of 60 and 70 units were considered for this first study. From the results obtained, it can be inferred that the usage of the relation $E \propto \rho^m$, where E is the Young's modulus of the macroscopic porous material, ρ is the density, and m is a power-scaling exponent, may remain valid. This is because it concerns the linear elastic region, where Figure 6 shows that the pore-structure is less

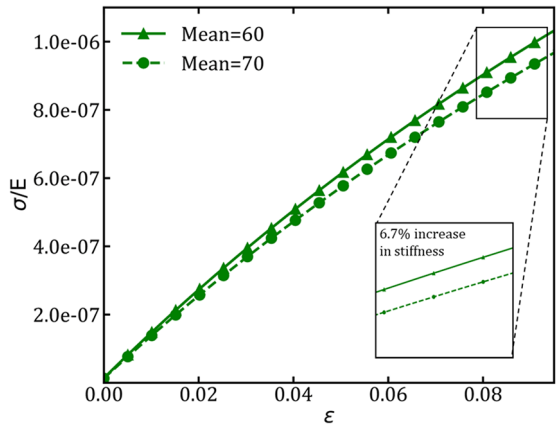

Figure 6. Effect of varying the mean pore-width on the macroscopic stress-strain response for open-porous material for given constant solid fraction (relative density) and pore-wall thickness.

influential. However, beyond this region, density no longer remains the critical factor controlling the mechanical properties. This becomes particularly important for flexible porous materials which posses a respectable recovery upon unloading after compression. Developing theoretical models by only focusing on the density may not help realise the complete picture in case of poly-disperse open-porous cellular materials.

4. Conclusion

In conclusion, the relative density, the pore-wall thickness and also the pore-size distribution together dictate the mechanical properties of open-porous cellular materials. The proposed computational method validates the previously published analysis on the effect of the mean pore-size and the broadness of the pore-size distribution on the macroscopic mechanical response considering micromechanical constitutive models. As can be inferred from the results, although the relative density plays a more important role in the linear elastic region, the effect of the pore-size distribution and pore-wall thickness cannot be neglected, especially while simulating a poly-disperse microstructure. Thus, the pore-sizes and their role in dictating the mechanical properties of open-porous cellular materials and the necessity for them to be accounted for while synthesising such materials for relevant mechanical load-bearing applications become less insignificant. Further investigations are necessary to support the first results from this study.

Funding

The author(s) disclosed receipt of the following financial support for the research, authorship, and/or publication of this article: This work has been funded by the Programme Directorate Transport of the German Aerospace Centre (Road Traffic Project "FFAE"). Furthermore, S. Aney acknowledges the DLR-DAAD Research Fellowship Programme.

ORCID iD

Ameya Rege https://orcid.org/0000-0001-9564-5482

References

[1] Gibson, LJ. Cellular solids. *Mrs Bulletin* 2003; 28(4): 270–274.
[2] Duarte, I, Peixinho, N, Andrade-Campos, A, et al. Special issue on cellular materials. *Sci Technol Mater* 2018; 30(1): 1–3.
[3] Peixinho, N, Duarte, I, Campos, AA, et al. *Cellular materials: structural behaviour, modelling and characterisation*. Aveiro: Universidade de Aveiro, 2017.
[4] Liu, P, and Chen, GF. *Porous materials: processing and applications*. Waltham, MA: Elsevier, 2014.

[5] Degischer, HP, and Kriszt, B. *Handbook of cellular metals (Vol. 71)*. Weinheim: Wiley-VCH, 2002.
[6] Öchsner, A, Murch, GE, and de Lemos, MJ. *Cellular and porous materials: thermal properties simulation and prediction*. Weinheim: John Wiley Sons, 2008.
[7] Hrubesh, LW. Aerogel applications. *J Non-Cryst Solids* 1998; 225: 335–342.
[8] Randall, JP, Meador, MA, and Jana, SC. Tailoring mechanical properties of aerogels for aerospace applications. *ACS Appl Mater Interfaces* 2011; 3(3): 613–626.
[9] Ratke, L, and Milow, B. *Aerogels for foundry applications*. New York: Springer, 2011.
[10] Hrubesh, LW, and Pekala, RW. Thermal properties of organic and inorganic aerogels. *J Mater Res* 1994; 9(3): 731–738.
[11] Lutz, MP, and Zimmerman, RW. The effect of pore shape on the Poisson ratio of porous materials. *Math Mech Solids* 2021; 26(8): 1191–1203.
[12] Langlois, V, Trinh, V, Lusso, C, et al. Permeability of solid foam: effect of pore connections. *Phys Rev E* 2018; 97(5): 053111.
[13] Song, S, Ding, Q, and Wei, J. Improved algorithm for estimating pore size distribution from pore space images of porous media. *Phys Rev E* 2019; 100(5): 053314.
[14] Hertel, SA, Wang, X, Hosking, P, et al. Magnetic-resonance pore imaging of nonsymmetric microscopic pore shapes. *Phys Rev E* 2015; 92(1): 012808.
[15] Bakhshian, S, and Sahimi, M. Computer simulation of the effect of deformation on the morphology and flow properties of porous media. *Phys Rev E* 2016; 94(4): 042903.
[16] Kraynik, AM. The structure of random foam. *Adv Eng Mater* 2006; 8(9): 900–906.
[17] Kraynik, AM, Reinelt, DA, and van Swol, F. Structure of random monodisperse foam. *Phys Rev E* 2003; 67(3): 031403.
[18] Jang, WY, Kraynik, AM, and Kyriakides, S. On the microstructure of open-cell foams and its effect on elastic properties. *Int J Solids Struct* 2008; 45(7–8): 1845–1875.
[19] Jang, WY, Kyriakides, S, and Kraynik, AM. On the compressive strength of open-cell metal foams with Kelvin and random cell structures. *Int J Solids Struct* 2010; 47(21): 2872–2883.
[20] Zhu, H, Hobdell, J, and Windle, A. Effects of cell irregularity on the elastic properties of 2D Voronoi honeycombs. *J Mech Phys Solids* 2001; 49(4): 857–870.
[21] Zhu, H, Thorpe, S, and Windle, A. The effect of cell irregularity on the high strain compression of 2D Voronoi honeycombs. *Int J Solids Struct* 2006; 43(5): 1061–1078.
[22] Rege, A, Hillgärtner, M, and Itskov, M. Mechanics of biopolymer aerogels based on microstructures generated from 2-d Voronoi tessellations. *J Supercri Fluid* 2019; 151: 24–29.
[23] Li, K, Gao, XL, and Subhash, G. Effects of cell shape and strut cross-sectional area variations on the elastic properties of three-dimensional open-cell foams. *J Mech Phys Solids* 2006; 54(4): 783–806.
[24] Gibson, L, and Ashby, M. *Cellular solids: structure and properties*. London: University of Cambridge, 1999.
[25] Rege, A, Aney, S, and Milow, B. Influence of pore-size distributions and pore-wall mechanics on the mechanical behavior of cellular solids like aerogels. *Phys Rev E* 2021; 103(4): 043001.
[26] Rege, A. Constitutive modeling of the densification behavior in open-porous cellular solids. *Materials* 2021; 14(11): 2731.
[27] Hill, R. Elastic properties of reinforced solids: some theoretical principles. *J Mech Phys Solids* 1963; 11(5): 357–372.
[28] Guedes, J, and Kikuchi, N. Preprocessing and postprocessing for materials based on the homogenization method with adaptive finite element methods. *Comput Methods Appl Mech Eng* 1990; 83(2): 143–198.
[29] Liu, C. On the minimum size of representative volume element: an experimental investigation. *Exp Mech* 2005; 45(3): 238–243.
[30] Kanit, T, Forest, S, Galliet, I, et al. Determination of the size of the representative volume element for random composites: statistical and numerical approach. *Int J Solids Struct* 2003; 40(13–14): 3647–3679.
[31] Gusev, AA. Representative volume element size for elastic composites: a numerical study. *J Mech Phys Solids* 1997; 45(9): 1449–1459.
[32] Okuma, G, Kadowaki, D, Shinoda, Y, et al. Determination of the size of representative volume element for viscous sintering. *J Ceram Soc Japan* 2016; 124(4): 421–425.
[33] Shan, Z, and Gokhale, AM. Representative volume element for non-uniform micro-structure. *Comp Mater Sci* 2002; 24(3): 361–379.
[34] Chandrasekaran, R, Hillgärtner, M, Ganesan, K, et al. Computational design of biopolymer aerogels and predictive modelling of their nanostructure and mechanical behaviour. *Sci Rep* 2021; 11(1): 10198.
[35] Vasseur, J, Wadsworth, FB, Coumans, JP, et al. Permeability of packs of polydisperse hard spheres. *Phys Rev E* 2021; 103(6): 062613.
[36] Bezrukov, A, Bargieł, M, and Stoyan, D. Statistical analysis of simulated random packings of spheres. *Part Part Syst Charact* 2002; 19(2): 111–118.
[37] Lubachevsky, BD, and Stillinger, FH. Geometric properties of random disk packings. *J Stat Phys* 1990; 60(5): 561–583.
[38] Baranau, V, Hlushkou, D, Khirevich, S, et al. Pore-size entropy of random hard-sphere packings. *Soft Matter* 2013; 9(12): 3361–3372.

[39] Mościński, J, Bargieł, M, Rycerz, Z, et al. The force-biased algorithm for the irregular close packing of equal hard spheres. *Mol Simul* 1989; 3(4): 201–212.
[40] Baranau, V, and Tallarek, U. Random-close packing limits for monodisperse and polydisperse hard spheres. *Soft Matter* 2014; 10(21): 3826–3841.
[41] Aurenhammer, F, and Klein, R. Voronoi diagrams. In: Sack JR and Urrutia J (eds) *Handbook of computational geometry*. Amsterdam: Elsevier, 2000, pp.201–290.
[42] Imai, H, Iri, M, and Murota, K. Voronoi diagram in the laguerre geometry and its applications. *SIAM J Comp* 1985; 14(1): 93–105.
[43] Alsayednoor, J, and Harrison, P. Evaluating the performance of microstructure generation algorithms for 2-d foam-like representative volume elements. *Mech Mater* 2016; 98: 44–58.
[44] Kraynik, AM. Foam structure: from soap froth to solid foams. *MRS Bull* 2003; 28(4): 275–278.
[45] Warren, WE, and Kraynik, AM. The nonlinear elastic behavior of open-cell foams. *J Appl Mech* 1991; 58(2): 376–381.
[46] Davini, C, and Ongaro, F. A homogenized model for honeycomb cellular materials. *J Elast* 2011; 104(1–2): 205–226.
[47] Rege, A, Schestakow, M, Karadagli, I, et al. Micro-mechanical modelling of cellulose aerogels from molten salt hydrates. *Soft Matter* 2016; 12(34): 7079–7088.
[48] Wu, W, Owino, J, Al-Ostaz, A, et al. Applying periodic boundary conditions in finite element analysis. In: *SIMULIA community conference, providence*. pp. 707–719, https://imechanica.org/files/pbc.pdf
[49] Jang, WY, and Kyriakides, S. On the crushing of aluminum open-cell foams: part II analysis. *Int J Solids Struct* 2009; 46(3–4): 635–650.